ISAS - INTERNATIONAL SCHOOL FOR ADVANCED STUDIES

Stability of alpha-phases on semiconductor surfaces

Master's thesis

Gerardo Ballabio

Supervisors: S. Scandolo, E. Tosatti

Academic year: 1997/98

SISSA - SCUOLA INTERNAZIONALE SUPERIORE DI STUDI AVANZATI

TRIESTE
Via Beirut 2-4

TRIESTE

Contents

Introduction

The importance of semiconductor devices in modern technology can be hardly overestimated. Since the invention of transistors in 1947, they have been widely used in every kind of electronic circuitry. The characterization of semiconductor materials is then a fundamental subject in many fields of physics and industry.

Semiconductor interfaces deserve a special attention. The presence of an interface breaks the full translational simmetry of the system, thus altering the resulting band structure. It is well known that, in this case, so-called *interface states* appear, i.e., states whose wavefunctions are localized in a very small region (only few atomic layers thick) surrounding the interface. These states usually place themselves in the gap between the valence and conduction bands; often they are half-filled, giving the system a metallic character.

Surfaces are a special case of this situation. It is found that surfaces of most materials *reconstruct*, i.e., atoms near the surface rearrange their positions in a configuration energetically more favoured than that they would have in the bulk (such a configuration is called a *reconstruction*). This phenomenon is particularly strong in semiconductors, in which atoms are tied together by covalent bonds; usually there is a hybridization of atomic states, producing sp^2 and/or sp^3 orbitals. Such orbitals are strongly directional, and at a surface, some of them point outward and don't form bonds with other atoms: these are the so-called *dangling bonds*. The presence of dangling bonds is energetically unfavourable, so atoms find more convenient to rearrange their geometry to reduce the number of them.

There are usually different competing reconstructions, consisting in different spatial configurations of the surface atoms; they induce different surface states, and can modify the character of the system from insulator to metallic or vice-versa. Determining the reconstructions of surfaces of a given material is therefore a very important subject in the study of semiconductors, as it represents the first basic step to the understanding of single-crystal growth and interface formation.

In the case of single-crystal growth, we deal with clean surfaces. There are many ways in which a clean surface can reconstruct; tipically this causes only the first one or two atomic layers to change significantly their geometry, while a few deeper layers are slightly distorted. An important reconstruction mechanism is the formation of *adatoms*, i.e., single atoms placed over a complete layer of atoms. Adatoms hybridized sp^3, such as those of diamond-structure semiconductors, usually lie over the site midway among three surface atoms *saturating* their dangling bonds, i.e., pairing each of them to an orbital of theirs, thus turning them into covalent bonds (this can be done with relatively little distortion of the orbitals); this way, three dangling bonds are removed while only one is formed, namely, the fourth sp^3 orbital of the adatom.

Another subject of interest is the deposition of one substance on another: this is a widely used technique to produce a clean surface of a given material over a suitable substrate. This starts with the deposed atoms being *adsorbed* by the surface, i.e., binding themselves to the surface as adatoms. The reconstructions of such surfaces depend on both the adsorbate (i.e., the adsorbed material) and the substrate, and also on the coverage rate, i.e., the surface density of adsorbed atoms. The coverage rate is usually measured in *monolayers*: 1 monolayer is the number of atoms per layer of the clean (unreconstructed) surface.

A widely studied case is that of semiconductors having a diamond structure, namely carbon (C) in the diamond phase, silicon (Si), germanium (Ge) and the alpha phase of tin (α-Sn). Sn, in fact, presents two solid phases called α (grey tin) and β (white tin; a third phase, γ-Sn, appears only at very high pressures); only the former has a diamond structure, while the latter doesn't behave as a semiconductor either.

On the (111) surface of a diamond-structure substance, a possible reconstruction is the so-called α phase, in which adatoms cover all the surface atoms' dangling bonds. The density of adatoms is then 1/3 monolayer, and the number of dangling bonds is correspondingly reduced. Such a reconstruction is also called a $\sqrt{3} \times \sqrt{3}$ R30^0 ($\sqrt{3}$ for brevity), due to the shape of the unit cell: see figure 2.2. An α phase is observed, for example, for Sn-Ge(111) (i.e., Sn atoms adsorbed on a Ge (111) surface), Sn-Si(111), and Pb-Ge(111) systems; it is not observed, instead, in clean Si(111) and Ge(111) systems.

In this work, we use first-principles calculations to analyse the reasons of such a behavior. Calculations are performed on the Sn-Ge(111) surface: the $\sqrt{3}$ reconstruction is compared to the competing 2×2 one (see again figure 2.2), as both are observed experimentally. The same reconstructions are also studied, for comparison, for a clean Ge(111) surface. In Chapter 1 the computational method is briefly exposed, while in Chapter 2 the systems studied are described in detail. Results are presented and discussed in Chapter 3.

Chapter 1

Computational methods

1.1 The PWSCF (plane-wave self-consistent field) method

In the framework of the density-functional theory (DFT) [1, 2, 3], the problem of solving the Hamiltonian of a solid can be reduced to a system of the so-called Kohn-Sham equations [2]:

$$\begin{aligned} H_{KS}\phi_i(\mathbf{r}) &= \left(-\frac{1}{2}\nabla^2 + V(\mathbf{r}) + \int \frac{n(\mathbf{r}')}{|\mathbf{r}-\mathbf{r}'|}d\mathbf{r}' + V_{xc}(\mathbf{r}')\right)\phi_i(\mathbf{r}) = \varepsilon_i\phi_i(\mathbf{r}) \\ n(\mathbf{r}) &= \sum_i \theta(\varepsilon_i - \varepsilon_F)|\phi_i(\mathbf{r})|^2 \end{aligned}$$

where the $\phi_i(\mathbf{r})$ are called single-particle orbitals; $n(\mathbf{r})$ is the total electron density and $V(\mathbf{r})$ the potential generated by nuclei (possibly plus an external potential), while $V_{xc}(\mathbf{r})$ is called the exchange-correlation potential. Its exact form cannot be calculated, but a number of approximations are available; for example in the Local Density Approximation (LDA) [2]

$$V_{xc}(\mathbf{r}) = \frac{\delta\left(n(\mathbf{r})\varepsilon_{xc}[n(\mathbf{r})]\right)}{\delta n(\mathbf{r})}$$

$\varepsilon_{xc}[n(\mathbf{r})]$ being the exchange-correlation energy of the system, that is a functional of $n(\mathbf{r})$ [1].

The Kohn-Sham equations are solved iteratively by choosing a trial expression for $n(\mathbf{r})$, obtaining $V_{xc}(\mathbf{r})$ from it, and then calculating a new expression for $n(\mathbf{r})$; the procedure is repeated until self-consistency is achieved.

In the plane-wave self-consistent field method [4], the single-particle orbitals are written as

$$\phi_{n\mathbf{k}}(\mathbf{r}) = \sum_{\mathbf{G}} e^{i(\mathbf{k}+\mathbf{G})\cdot\mathbf{r}} C_{n\mathbf{k}}(\mathbf{G})$$

where the $\mathbf{G}$'s are the reciprocal lattice vectors of the crystal, while $\mathbf{k}$ is a vector of the first Brillouin zone (BZ). The Kohn-Sham system is then solved for a finite number of equations, selected by choosing a finite set of $\mathbf{k}$'s in the BZ and by restricting to the plane waves $e^{i(\mathbf{k}+\mathbf{G})\cdot\mathbf{r}}$ such that $|\mathbf{k}+\mathbf{G}|$ is less than a given cutoff energy E_{cut}. Sets of so-called special k-points are available in literature [5, 6] that allow accurate results using a small number of $\mathbf{k}$'s.

This way, the system's wavefunctions are calculated *ab initio* for a given set of atomic positions. For the given configuration, the Hellmann-Feynman forces [4] acting on atoms can then be calculated, atoms be moved according to these forces, and the procedure repeated until the forces become less than a given value, or the energy of the system reaches a (possibly global) minimum.

Finally, given the wavefunctions, band energies and the total energy of the system are easily calculated.

1.2 Pseudopotentials

Especially in large atoms, electrons of the inner shells have very strong binding energies and very localized wavefunctions; a PWSCF calculation involving these electrons would then require a very large cutoff energy, and thus a very large number of plane waves (which grows roughly as $E_{\text{cut}}^{3/2}$), resulting in a very time- (and memory-) consuming calculation.

A substantial lowering of the cutoff required to obtain accurate results can be achieved by taking into account only electrons of the outer shells (i.e., valence electrons), while inner-shells electrons (also called core electrons) can be considered not to interact with other atoms; their wavefunctions can then be calculated by solving a single-atom Hamiltonian, and so does the screened potential that outer electrons see: this is called a pseudopotential.

Pseudopotentials can be calculated by solving the all-electrons single-atom problem, and then requiring that "pseudo-wavefunctions", i.e., wavefunctions of the pseudo-Hamiltonian, coincide with true valence wavefunctions outside a suitable "core radius" r_c; moreover, they must be sufficiently smooth to be accurately evaluated with a low cutoff.

A pseudopotential is said to be transferable, if it gives reliable results for different systems; another property that is usually required is norm-conservation [7], i.e., that integrals from 0 to r_c of real and pseudo-wavefunctions be equal for each valence state. It is found that to satisfy these requirements, pseudopotentials must be non-local, i.e., depend on the angular momentum of electrons; a computationally efficient form for non-local pseudopotentials is given in [8]. An extensive set of pseudopotentials can be found in [9].

1.3 Surface calculations

As PWSCF calculations are only affordable for a small number of atoms (with our computational facilities and using Sn and Ge atoms, we couldn't have more than about 50 of them, due to memory constraints), periodic boundary conditions are necessary to avoid unwanted surface effects; in calculations on bulk solids, the unit cell of the crystal is the natural choice. A surface system, however, doesn't have a translational simmetry in the direction orthogonal to the surface. Calculations are then done on a slab a few atomic layers thick, which has an upper and a lower surface; by imposing periodic boundary conditions, the system becomes an infinite sequence of repeating slabs.

While in directions parallel to the surface the periodic cell can be made as small as the surface reconstruction periodicity allows (down to a 1×1 cell, i.e., a single atom per layer, for unreconstructed surfaces), in the orthogonal direction the upper and lower surface must be sufficiently distant not to interact with each other, both in the same cell and in neighboring cells; this means that the slab must consist of a sufficiently large number of layers, and also that there must be enough empty space in the cell above and below the surfaces. The periodic cell has therefore the shape of a tall prism; the corresponding Brillouin zone is a very low one, so that two-dimensional sets of special points can be used.

The lower surface can be a replica of the upper one, in which case all quantities such as the surface energy must be divided by two; but a common technique is to leave it unreconstructed and to saturate its dangling bonds with hydrogen atoms. This way, the lower surface is like a truncated bulk, and does not influence the upper surface. When this choice is made, while atoms near the upper surface are allowed to move according to the Hellmann-Feynman forces, the lowest layers' atoms are also kept fixed in their bulk positions, which increases their "bulk-like" character.

In this work we did all calculations with the program `pwscf`, which implements the PWSCF method using the Ceperley-Alder exchange-correlation potential functional [10, 11]. Pseudopotentials of the Kleinman-Bylander form [8, 12] are used. The Davidson method [13] is used to solve the Kohn-Sham system in momentum space, and a modified Broyden algorithm [14] is used to accelerate convergence. Details on the unit cells, the cutoff, and the k-point samplings used are given in section 2.4.

Chapter 2

Systems studied

2.1 (111) surfaces: adatom sites

On the (111) surface of a diamond-structure crystal, there are two sets of inequivalent sites where adatoms can lie: either on the top of an underlying atom of the second surface layer, or over a hollow site of the same layer (in this case, the nearest underlying atom is one of the fourth layer), as shown in figure 2.1. The two positions are usually called T_4 (T stands for "top") and H_3 (H stands for "hollow"), respectively.

There is computational evidence [15, 16, 17] that T_4 sites are almost always energetically more favourable: in fact, the atom directly below the adatom can move inward to reduce stresses, while simmetry doesn't allow this in the H_3 geometry. In our calculations, therefore, we placed all adatoms in T_4 positions.

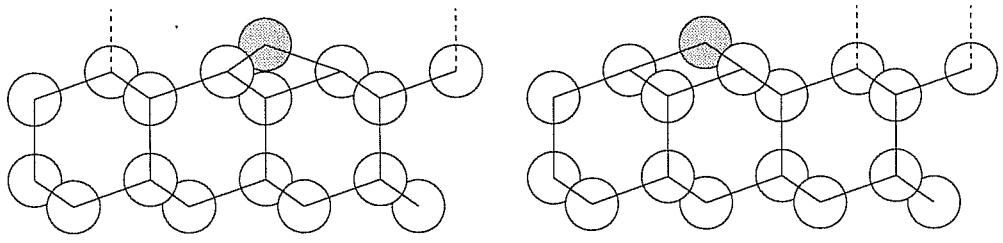

Figure 2.1: Side view of an adatom placed on: (a) a T_4 site. (b) an H_3 site. Adatoms are shaded in grey. Dashed lines represent dangling bonds.

2.2 Ge(111) and Sn-Ge(111) 2×2 reconstructions: the adatom-rest atom mechanism

2×2 reconstructions are so called because their unit cell has twice the side of an unreconstructed (111) surface, thus containing four atoms per layer. The structure of a 2×2 reconstruction is shown in figure 2.2. Such reconstructions are driven by the so-called *adatom-rest atom* mechanism: while three atoms per unit cell establish chemical bonds with the adatom, the fourth atom of the topmost layer (called a *rest atom*) has a dangling bond at a lower energy level than that of the adatom. A charge transfer (partial of total) then happens between them, thus making two half-filled states into a "mostly filled" and a "mostly empty" one: the total energy is lowered by this process.

In this work the Sn-Ge(111) 2×2 reconstruction, which is experimentally observed [18], was studied: in this system, the Sn coverage rate is 1 atom per 2×2 cell, or 1/4 monolayer. We also studied the Ge(111) 2×2 reconstruction, taking it as the lowest-energy reconstruction of this surface. Actually the experimentally observed reconstruction is the c(2×8) one [19, 20], which is shown in figure 2.3; but this surface, having a unit cell twice as large as the 2×2 one, is computationally too expensive. Because of the similarity between the two systems (the c(2×8) cell can be divided into a 2×2 and a c(4×2) subcells, whose surface energies are practically indistinguishable), we suppose their difference in energy to be sufficiently small.

2.3 Ge(111) and Sn-Ge(111) α ($\sqrt{3}$) reconstructions

In $\sqrt{3}$ reconstructions, all topmost-layer atoms establish chemical bonds with adatoms. The structure is shown in figure 2.2: the unit cell of such a reconstruction contains three atoms per layer, has a side $\sqrt{3}$ times larger than that of the 1×1 cell, and is rotated 30^0 with respect to it. The reconstruction is therefore called $\sqrt{3}\times\sqrt{3}$ R30^0 ($\sqrt{3}$ for brevity). As there is a single dangling bond per unit cell, the system must have a half-filled electron band; it is therefore a metal, while the 2×2 system, having two dangling bonds per cell (one of which is filled while the other is empty, as said above), is an insulator.

In this work the Sn-Ge(111) $\sqrt{3}$ reconstruction was studied: its Sn coverage rate is 1 atom per $\sqrt{3}$ cell, or 1/3 monolayer. Such a reconstruction is experimentally observed for this system [21, 22, 23, 24, 25], but is not for the Ge(111) one, which we also studied for comparison.

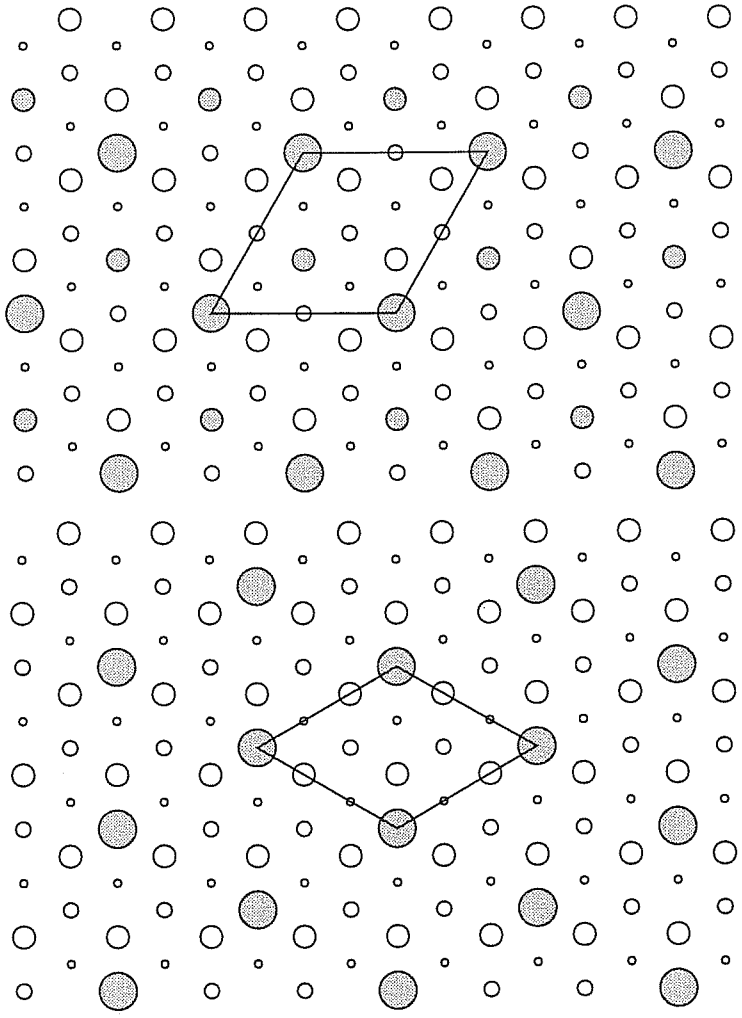

Figure 2.2: Top view of: (a) a 2×2 reconstruction; (b) a $\sqrt{3}$ reconstruction. The larger the circles, the higher the corrisponding atoms; adatoms are the largest circles at all. Adatoms and rest atoms, that is, atoms with dangling bonds, are shaded in grey. The unit cells are outlined.

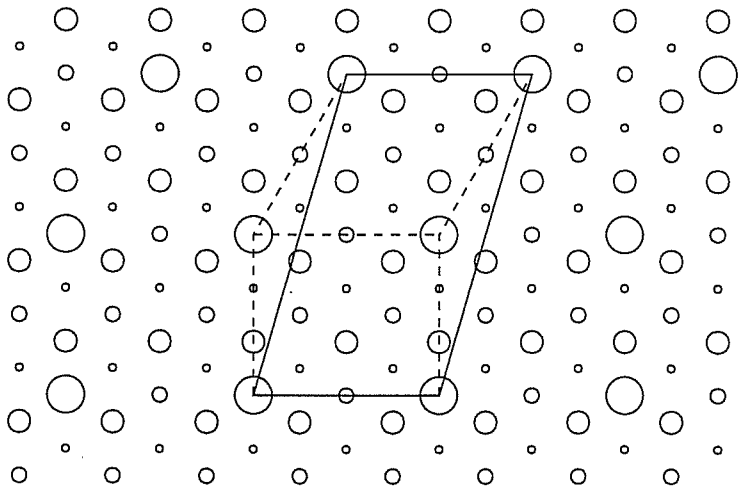

Figure 2.3: Top view of a c(2 × 8) reconstruction. The larger the circles, the higher the corrisponding atoms; adatoms are the largest circles at all. The unit cell is outlined in solid; the 2 × 2 and c(4 × 2) subcells are also shown with dashed lines.

2.4 Computational details

Before calculating the surfaces previously described, a cell of bulk Ge was examined to determine the optimal (i.e., minimum-energy) lattice spacing. The geometry of the cell was chosen to be similar to those used for the surface calculations: it had a 1 × 1 periodicity in the horizontal directions, thus containing one atom per layer, and consisted of 12 layers vertically (a number of layers not multiple of 6 would not allow vertical periodicity). The coordinates of the 12 Ge atoms, in units of the horizontal cell side a, are shown in table 2.1. We found an optimal cell side of 7.575 atomic units, the experimental value being 7.560 a.u. [26].

For our surface systems, we used a slab with the same horizontal periodicity of the reconstruction, namely 2 × 2 and $\sqrt{3} \times \sqrt{3}$ R30^0: there were therefore 4 and 3 atoms per layer, respectively. A 10-layers slab was used, with an adatom on the top surface, while the dangling bonds on the bottom surface were saturated with hydrogen atoms: the 10 Ge layers, plus the H one, plus the adatom, correspond to the 12 layers used in the cell described above. The total number of atoms per cell was then 45 for 2×2 systems, and 34 for $\sqrt{3}$ ones. The empty space between periodic images of the slab was about 20 atomic units, i.e., about 10 Å. The systems were relaxed allowing adatoms and atoms of the 6 topmost layers to move, while other layers were

coordinates			coordinates		
0.0000	0.0000	2.1433	0.0000	0.0000	-0.3062
0.5000	0.2887	1.9392	0.5000	0.2887	-0.5103
0.5000	0.2887	1.3268	0.5000	0.2887	-1.1227
-0.5000	-0.2887	1.1227	-0.5000	-0.2887	-1.3268
-0.5000	-0.2887	0.5103	-0.5000	-0.2887	-1.9392
0.0000	0.0000	0.3062	0.0000	0.0000	-2.1433

Table 2.1: Atomic positions for the bulk Ge slab. All coordinates are in units of the horizontal cell side = 7.57507 a.u. The vertical cell side is 37.1101 a.u.

	unrelaxed coords			relaxed, Sn-Ge			relaxed, Ge		
A	0.0000	0.0000	1.1196	0.0000	0.0000	1.2774	0.0000	0.0000	1.2492
	-0.1667	-0.2887	1.0017	-0.1539	-0.2666	1.0134	-0.1510	-0.2615	1.0142
	-0.1667	0.2887	1.0017	0.3078	0.0000	1.0134	0.3020	0.0000	1.0142
	0.3333	0.0000	1.0017	-0.1539	0.2666	1.0134	-0.1510	0.2615	1.0142
	-0.5000	-0.2887	0.8839	0.0000	0.0000	0.8392	0.0000	0.0000	0.8331
	0.0000	0.0000	0.8839	-0.5000	-0.2887	0.9168	-0.5000	-0.2887	0.9204
	0.5000	0.2887	0.8839	0.5000	0.2887	0.9168	0.5000	0.2887	0.9204
	-0.5000	-0.2887	0.5303	0.0000	0.0000	0.4933	0.0000	0.0000	0.4881
	0.0000	0.0000	0.5303	-0.5000	-0.2887	0.5493	-0.5000	-0.2887	0.5513
	0.5000	0.2887	0.5303	0.5000	0.2887	0.5493	0.5000	0.2887	0.5513
	-0.3333	0.0000	0.4125	0.1707	-0.2956	0.4152	0.1715	-0.2970	0.4152
	0.1667	-0.2887	0.4125	-0.3412	0.0000	0.4152	-0.3429	0.0000	0.4152
	0.1667	0.2887	0.4125	0.1707	0.2956	0.4152	0.1715	0.2970	0.4152
	-0.3333	0.0000	0.0589	-0.3369	0.0000	0.0593	-0.3373	0.0000	0.0592
	0.1667	-0.2887	0.0589	0.1685	-0.2918	0.0593	0.1686	-0.2921	0.0592
	0.1667	0.2887	0.0589	0.1685	0.2918	0.0593	0.1686	0.2921	0.0592
	-0.1667	-0.2887	-0.0589	-0.1657	-0.2870	-0.0585	-0.1655	-0.2867	-0.0590
	-0.1667	0.2887	-0.0589	-0.1657	0.2870	-0.0585	-0.1655	0.2867	-0.0590
	0.3333	0.0000	-0.0589	0.3314	0.0000	-0.0585	0.3311	0.0000	-0.0590
		...			...			...	
H	-0.3333	0.0000	-1.2283	-0.3333	0.0000	-1.2283	-0.3333	0.0000	-1.2283
H	0.1667	-0.2887	-1.2283	0.1667	-0.2887	-1.2283	0.1667	-0.2887	-1.2283
H	0.1667	0.2887	-1.2283	0.1667	0.2887	-1.2283	0.1667	0.2887	-1.2283

Table 2.2: Unrelaxed and relaxed atomic positions for the $\sqrt{3}$ slabs. The adatom is labelled A, the hydrogen atoms H. The four lowest Ge layers, which have been kept fixed, are not shown: they can be obtained by simmetries. All coordinates are in units of the horizontal cell side = 13.12041 a.u. The vertical cell side is 53.0255 a.u.

	unrelaxed coords			relaxed, Sn-Ge			relaxed, Ge		
A	0.0000	0.0000	0.9696	0.0000	0.0000	1.0692	0.0000	0.0000	1.0424
	-0.2500	-0.1443	0.8675	-0.2421	-0.1398	0.8570	-0.2386	-0.1378	0.8593
	0.0000	0.2887	0.8675	0.0000	0.2796	0.8570	0.0000	0.2755	0.8593
	0.2500	-0.1443	0.8675	0.2421	-0.1398	0.8570	0.2386	-0.1378	0.8593
R	0.5000	0.2887	0.8675	0.5000	0.2887	0.9422	0.5000	0.2887	0.9478
	-0.2500	-0.4330	0.7655	-0.2329	-0.4429	0.7878	-0.2316	-0.4436	0.7915
	0.0000	0.0000	0.7655	0.0000	0.0000	0.7202	0.0000	0.0000	0.7152
	0.2500	-0.4330	0.7655	0.2329	-0.4429	0.7878	0.2316	-0.4436	0.7915
	0.5000	0.0000	0.7655	0.5000	0.0198	0.7878	0.5000	0.0212	0.7915
	-0.2500	-0.4330	0.4593	-0.2510	-0.4325	0.4743	-0.2510	-0.4324	0.4771
	0.0000	0.0000	0.4593	0.0000	0.0000	0.4190	0.0000	0.0000	0.4167
	0.2500	-0.4330	0.4593	0.2510	-0.4325	0.4743	0.2510	-0.4324	0.4771
	0.5000	0.0000	0.4593	0.5000	-0.0011	0.4743	0.5000	-0.0012	0.4771
	-0.2500	0.1443	0.3572	-0.2577	0.1488	0.3576	-0.2583	0.1491	0.3584
	0.0000	-0.2887	0.3572	0.0000	-0.2976	0.3576	0.0000	-0.2983	0.3584
	0.2500	0.1443	0.3572	0.2577	0.1488	0.3576	0.2583	0.1491	0.3584
	0.5000	-0.2887	0.3572	0.5000	-0.2887	0.3673	0.5000	-0.2887	0.3690
	-0.2500	0.1443	0.0510	-0.2519	0.1455	0.0504	-0.2524	0.1457	0.0512
	0.0000	-0.2887	0.0510	0.0000	-0.2909	0.0504	0.0000	-0.2915	0.0512
	0.2500	0.1443	0.0510	0.2519	0.1455	0.0504	0.2524	0.1457	0.0512
	0.5000	-0.2887	0.0510	0.5000	-0.2887	0.0575	0.5000	-0.2887	0.0585
	-0.2500	-0.1443	-0.0510	-0.2509	-0.1449	-0.0496	-0.2508	-0.1448	-0.0488
	0.0000	0.2887	-0.0510	0.0000	0.2897	-0.0496	0.0000	0.2896	-0.0488
	0.2500	-0.1443	-0.0510	0.2509	-0.1449	-0.0496	0.2508	-0.1448	-0.0488
	0.5000	0.2887	-0.0510	0.5000	0.2887	-0.0543	0.5000	0.2887	-0.0544
		...			...			...	
H	-0.2500	0.1443	-1.0637	-0.2500	0.1443	-1.0637	-0.2500	0.1443	-1.0637
H	0.0000	-0.2887	-1.0637	0.0000	-0.2887	-1.0637	0.0000	-0.2887	-1.0637
H	0.2500	0.1443	-1.0637	0.2500	0.1443	-1.0637	0.2500	0.1443	-1.0637
H	0.5000	-0.2887	-1.0637	0.5000	-0.2887	-1.0637	0.5000	-0.2887	-1.0637

Table 2.3: Unrelaxed and relaxed atomic positions for the 2×2 slabs. The adatom is labelled A, the rest atom R, the hydrogen atoms H. The four lowest Ge layers, which have been kept fixed, are not shown: they can be obtained by simmetries. All coordinates are in units of the horizontal cell side = 15.15014 a.u. The vertical cell side is 53.0255 a.u.

system	k-points	weights
surfaces	(0.380718, 0, 0)	1
bulk Ge	(0.190359, 0, 0)	1/4
	(0.595180, 0.123819, 0)	1/4
	(0.404820, 0.123819, 0)	1/2

Table 2.4: 1- and 3-k-points sets used for calculations. Coordinates are in units $2\pi/a$, a being the horizontal cell side.

k-points	weights
(0.111111, 0.064150, 0)	1/9
(0.222222, 0.128300, 0)	1/9
(0.444444, 0.256600, 0)	1/9
(0.333333, 0.064150, 0)	2/9
(0.444444, 0.128300, 0)	2/9
(0.555556, 0.064150, 0)	2/9

Table 2.5: The 6-k-points set used for calculations. Coordinates are in units $2\pi/a$, a being the horizontal cell side.

kept fixed. Relaxed and unrelaxed atomic coordinates are shown in tables 2.2 and 2.3.

The energy cutoff for all calculations was 12 Ry, that had been previously determined to be the optimal choice for this kind of systems [12].

As of the k-points sampling, we first used the sets of k-points shown in table 2.4. A single point was used for the four surface systems to minimize the computation time, especially for the calculation of equilibrium positions: the special point of [6] was used, while the three-points sets used for the bulk Ge cell were obtained by refolding the 2×2 point over the 1×1-cell irreducible Brillouin zone (IBZ).

After relaxing atomic positions, total energy calculations were repeated with a better sampling of the IBZ, using for all three systems the 6-k-points sampling of [6]; some test calculations with an 18 k-points sampling (see again [6]) were also done. These points are shown in tables 2.5 and 2.6. Since, atomic positions were kept fixed to those determined by calculations with a single k-point: we tested that relaxing positions with three k-points gave negligible differences.

For our purposes we also needed to calculate the energy per atom of bulk Ge and Sn: we calculated the latter using a 2-atoms fcc cell (the crystal

k-points	weights	k-points	weights
(0.074074, 0, 0)	1/27	(0.185185, 0.064150, 0)	2/27
(0.148148, 0, 0)	1/27	(0.259259, 0.064150, 0)	2/27
(0.296296, 0, 0)	1/27	(0.407407, 0.064150, 0)	2/27
(0.370370, 0, 0)	1/27	(0.481481, 0.064150, 0)	2/27
(0.518519, 0, 0)	1/27	(0.296296, 0.128300, 0)	2/27
(0.592593, 0, 0)	1/27	(0.370370, 0.128300, 0)	2/27
(0.629630, 0.064150, 0)	1/27	(0.518519, 0.128300, 0)	2/27
(0.592593, 0.128300, 0)	1/27	(0.407407, 0.192450, 0)	2/27
(0.518519, 0.256600, 0)	1/27	(0.481481, 0.192450, 0)	2/27

Table 2.6: The 18-k-points set used for calculations. Coordinates are in units $2\pi/a$, a being the horizontal cell side.

coordinates	0.0000	0.0000	0.0000	0.2500	0.2500	0.2500

Table 2.7: Atomic positions for the 2-atoms fcc cells. All coordinates are in units of the cell side, that is 10.722 a.u. for Ge and 12.250 a.u. for Sn.

structure being that of diamond), having determined previously the optimal (i.e., minimum-energy) lattice spacing to be 12.250 a.u., compared with the experimental value of 12.267 a.u. [26]. The energy per Sn atom was -7.1476 Ry. The atomic coordinates are reported in table 2.7, while the special-k-points set used [5, 27] is reported in table 2.8.

For the Ge system, instead, we used the total energy, divided by 12, of our bulk Ge cell; however, for comparison we also considered a 2-atoms cell with Ge atoms, with a lattice spacing of 10.722 a.u., while the experimental result is 10.691 a.u. [26]. The energy per Ge atom was -8.0288 Ry, almost identical to the 12-atoms-cell result of -8.0291 Ry (using 6 k-points).

k-points	weights	k-points	weights
(0.125, 0.125, 0.125)	1/32	(0.125, 0.375, 0.625)	6/32
(0.125, 0.125, 0.375)	3/32	(0.125, 0.375, 0.875)	6/32
(0.125, 0.125, 0.625)	3/32	(0.125, 0.625, 0.625)	3/32
(0.125, 0.125, 0.875)	3/32	(0.375, 0.375, 0.375)	1/32
(0.125, 0.375, 0.375)	3/32	(0.375, 0.375, 0.625)	3/32

Table 2.8: The 10-k-points set used for calculations. Coordinates are in units $2\pi/a$, a being the fcc cell side.

Chapter 3

Results and discussion

3.1 Free energies and chemical potentials

Since the Sn coverage rate is not equal for all the systems we studied, the quantity we must consider to determine which reconstruction is energetically more favourable, is the free energy $\Omega = E - \mu N$ per surface unit area, where N is the number of Sn atoms: as we calculated energies E per 1×1-cell, N is 1/4 and 1/3 for Sn-Ge(111) 2×2 and $\sqrt{3}$ respectively, and 0 for Ge(111) reconstructions. The number of Ge atoms, instead, can be considered constant, provided we subtract the energy of 1 bulk Ge atom from that of Ge(111) cells (see section 2.4): in these slabs, in fact, there is one more Ge atom than in Sn-Ge(111) ones, that is, the adatom, and an atom "comes" from the bulk to fill the cell. This is equivalent to saying that the chemical potential for Ge is fixed to that of the bulk.

A physical constraint also applies to the Sn chemical potential: our surface reconstructions can't be equilibrium states (i.e., local minima of the free energy) if the chemical potential is greater than the energy of a Sn bulk atom [28, 29, 16]. If this were the case, the recontruction would be unstable against aggregation of Sn atoms in "drops" of bulk Sn. This upper bound to the Sn chemical potential, as calculated in section 2.4, is -7.1476 Ry.

The energies E are directly output by the program `pwscf` for the slabs considered. We first did all calculations using the 1- and 6-k-points sets of section 2.4 to sample the IBZ; then, because of the non-negligible difference between the two sets of results, we also did calculations with a 18-k-points set (also reported in section 2.4); we found energies very similar to those obtained with 6 k-points, indicating that convergence in k-point sampling was achieved with 6 k-points. Results are shown in table 3.1 and figure 3.1.

According to our results, there are two reconstructions that have the

system	k-points	slab energy	1×1-cell energy
bulk Ge	3	-96.37262 Ry	—
	6	-96.34938 Ry	—
	18	-96.34863 Ry	—
Sn-Ge 2×2	1	-332.60982 Ry	-83.15246 Ry
	6	-332.52724 Ry	-83.13181 Ry
	18	-332.52742 Ry	-83.13186 Ry
Sn-Ge $\sqrt{3}$	1	-251.26994 Ry	-83.75665 Ry
	6	-251.19178 Ry	-83.73059 Ry
	18	-251.19117 Ry	-83.73039 Ry
Ge 2×2	1	-333.46806 Ry	-81.35925 Ry
	6	-333.38601 Ry	-81.33922 Ry
	18	-333.38619 Ry	-81.33929 Ry
Ge $\sqrt{3}$	1	-252.12337 Ry	-81.36411 Ry
	6	-252.04485 Ry	-81.33858 Ry
	18	-252.04421 Ry	-81.33839 Ry

Table 3.1: Total energies E of the slabs considered. The energy of 1 Ge bulk atom (calculated with the corresponding number of k-points) has been subtracted from the Ge reconstructions energies to calculate the 1×1-cell energies.

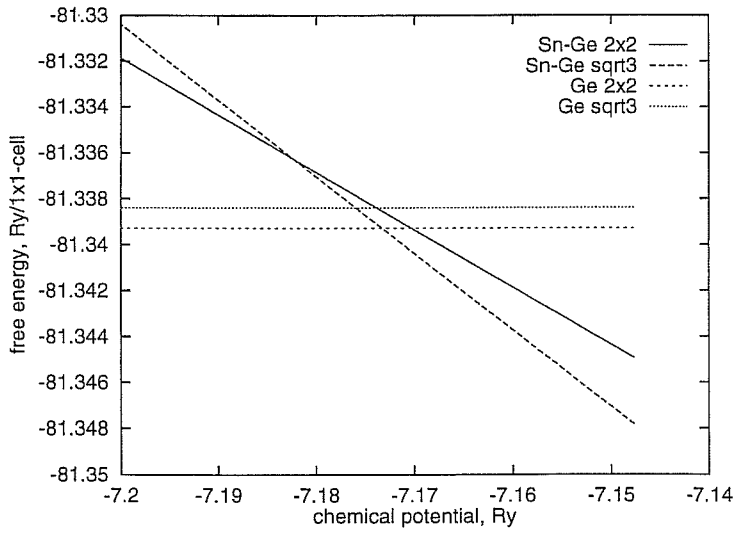

Figure 3.1: Free energies $\Omega = E - \mu N$ (N is the number of Sn atoms) per 1×1-cell of the systems considered, calculated with 18 k-points, as a function of the chemical potential μ. Lines end at the upper-bound value of $\mu = 7.1476$ Ry.

minimum value of Ω for some value of μ, i.e., the Sn-Ge $\sqrt{3}$ one (α phase) for -7.1733 Ry $< \mu < -7.1476$ Ry, and the Ge 2×2 one for $\mu < -7.1733$ Ry. This is only partially consistent with experimental evidence. Our results agree with experiment in predicting a stable α-phase for Sn-Ge(111) [21, 22, 23, 24, 25], but not for clean Ge(111), where, as expected, the 2×2 reconstruction is found to win over the $\sqrt{3}$ one [19, 20]. Instead, the 2×2 reconstruction, which has also been recently observed [18], should never exist according to our results. It has to be noticed, however, that the difference in the free energy between this reconstruction and the minimum-Ω one is very little (less than 1 mRy for the value of μ at which Sn-Ge $\sqrt{3}$ coexists with Ge 2×2) and therefore we can speculate that the 2×2 reconstruction may exist as a metastable one.

3.2 Bond angles and atomic hybridization

In table 3.2 the angles (with respect to the horizontal direction) and lengths of the adatoms' and rest atoms' bonds with their nearest neighbors in the various reconstructions are reported: we see that in all cases adatoms and rest atoms move considerably outward, thus increasing bond angles (see figure 3.2) with respect to the ideal tetrahedral value of 19.5^0. A mechanism that induces the raising of adatoms is surely the repulsion between each adatom and its underlying second-layer atom, since their distance is only 2/3 of the bulk bond length when they are in their unrelaxed positions.

Another mechanism, that is of interest for our problem, is the following. In sp^3 hybridization, atomic orbitals are a linear combination of the s and the three p wavefunctions, and the energies of the hybridized states are also linear combinations of ε_s and ε_p (namely, $(\varepsilon_s + 3\varepsilon_p)/4$ in the ideal case). When the bond angles are varied, the coefficients of the combinations also vary; in particular, it can be shown [30] that the energy of the dangling bond state is

$$E = \varepsilon_p - \frac{9}{4}(\varepsilon_p - \varepsilon_s)\sin^2\theta$$

The extrema of this situation are the cases $\sin\theta = 2/3$ ($\theta = 41.8^0$), in which $E = \varepsilon_s$, and $\theta = 0$, in which $E = \varepsilon_p$: in the former there is no hybridization at all, so that the three bonds are p orbitals and the dangling bond is an s one, while in the latter the three bonds are hybridized sp^2 and the dangling bond is the remaining p orbital. The tetrahedral case, in which all four orbitals have the same energy $(\varepsilon_s + 3\varepsilon_p)/4$, corresponds to the value $\sin\theta = 1/3$ ($\theta = 19.5^0$).

Because of this mechanism, as adatoms and rest atoms move outward,

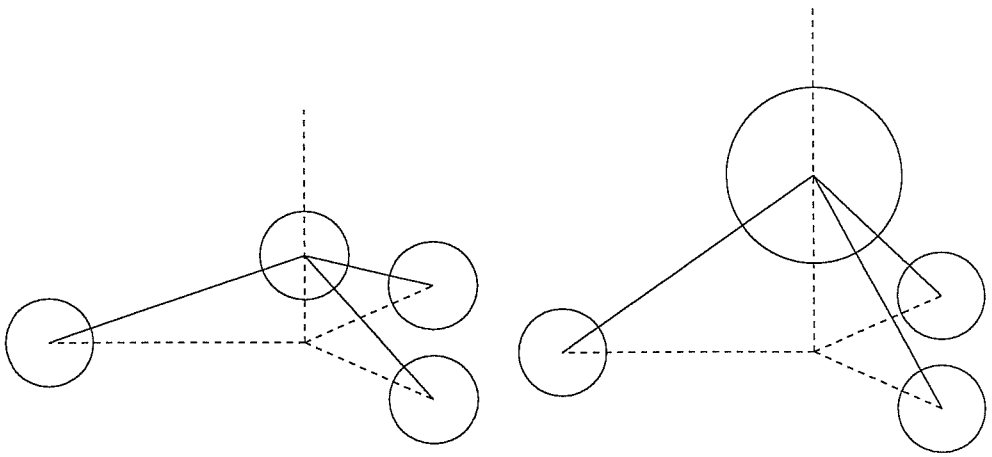

Figure 3.2: Bond angles between adatoms or rest atoms and their nearest neighbors. When bond lengths are larger (as in the case of larger adatoms), bond angles are also larger. The dashed lines pointing upward represent the dangling bonds.

system	bond angle	bond length	2nd-layer dist.
ideal (tetrahedral)	19.5^0	4.639 a.u.	3.093 a.u.
Sn-Ge using covalent radii	28.6^0	4.981 a.u.	3.930 a.u.
ideal bond length	—	—	4.639 a.u.
ideal bond length, Sn-Ge	—	—	4.981 a.u.
Sn-Ge $\sqrt{3}$, adatom	40.6^0	5.321 a.u.	5.749 a.u.
Sn-Ge 2×2, adatom	37.2^0	5.317 a.u.	5.281 a.u.
Sn-Ge 2×2, rest atom	29.9^0	4.698 a.u.	—
Ge $\sqrt{3}$, adatom	37.9^0	5.021 a.u.	5.460 a.u.
Ge 2×2, adatom	33.6^0	5.012 a.u.	4.957 a.u.
Ge 2×2, rest atom	30.3^0	4.693 a.u.	—

Table 3.2: Bond angles and lengths for adatoms and rest atoms for the reconstructions studied. The ideal (tetrahedral) value, and the value obtained by using the Sn-Ge covalent bond length, are given for comparison. The adatoms' distances from the underlying 2nd-layer atoms are also reported and compared with the ideal values.

surface bands of their dangling bonds lower their energies, thus "stabilizing" the system. A clear evidence that rehybridization is energetically more important than repulsion is given by the fact that rest atoms, that have no underlying neighboring atom so that the repulsive mechanism doesn't apply, also raise considerably their positions (see table 3.2).

A simple geometrical argument that explains the different behavior of clean and Sn-covered Ge(111) surfaces can now be straightforwardly formulated. The larger size of the Sn adatom (see figure 3.2) naturally favours a larger bond angle with respect to a Ge adatom. The covalent radius for Sn is in fact 1.40 Å, to be compared with 1.22 Å for Ge.

Since the $\sqrt{3}$ surface is stabilized by the outward motion of the adatom, that we know to be more favourable for Sn, while the 2×2 one is stabilized by that of the rest atom, which is a Ge atom for both Sn-covered and clean Ge(111), we thus conclude that a simple argument based on the different atomic size of Sn and Ge nicely accounts for the markedly different behavior of the two surfaces.

In support of the above argument, we show in figures 3.3 and 3.4 the electron bands of the four surface reconstructions. Surface bands are clearly seen: in $\sqrt{3}$ reconstructions we have one of these, that corresponds to the adatoms' dangling bonds, while in 2×2 ones there are two surface bands, that correspond to the adatoms' (the higher one) and to the rest atoms' (the lower one) dangling bonds. We have verified these correspondences by calculating the spatial charge density of the states: results are shown in figure 3.6.

For both kinds of reconstructions, we can observe a lowering of the adatoms' dangling-bond bands, and of the Fermi energy, for Sn-Ge systems with respect to Ge ones, in agreement with the simple picture given above. This gives the Sn adatom's dangling bond a more *s*-like character, thus lowering the energy of the corresponding band.

The mechanism applies to $\sqrt{3}$ and 2×2 reconstructions differently: in the formers, the adatom's dangling-bond band is half-occupied, so that by lowering its energy, the total energy of the system is also lowered. We therefore expect for $\sqrt{3}$ adatoms a strong tendency to move outward. In the latters, instead, by moving the rest atom outward, its dangling-bond band, that is fully occupied, lowers its energy, thus reducing the total energy; but by moving outward the adatom, the lowering of its dangling-bond band, that is empty, doesn't contribute to decrease the total energy. We then expect for 2×2 adatoms a weaker tendency to move outward than for $\sqrt{3}$ ones. In fact, we can see from table 3.2 that bond angles in $\sqrt{3}$ systems are actually larger (about 3–4 degrees) than in 2×2 ones.

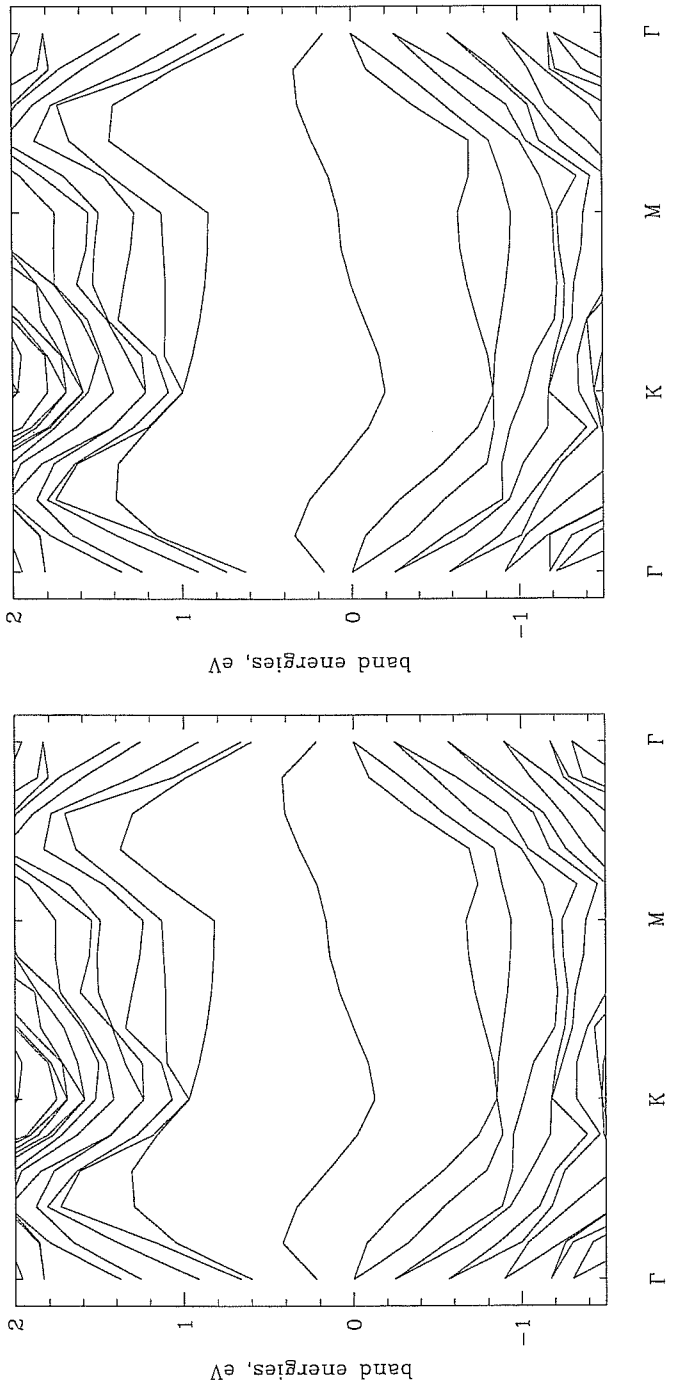

Figure 3.3: (a) Sn-Ge $\sqrt{3}$ electron bands; (b) Ge $\sqrt{3}$ ones. The region around the Fermi energy is shown. Plots are rotated to allow a better comparison.

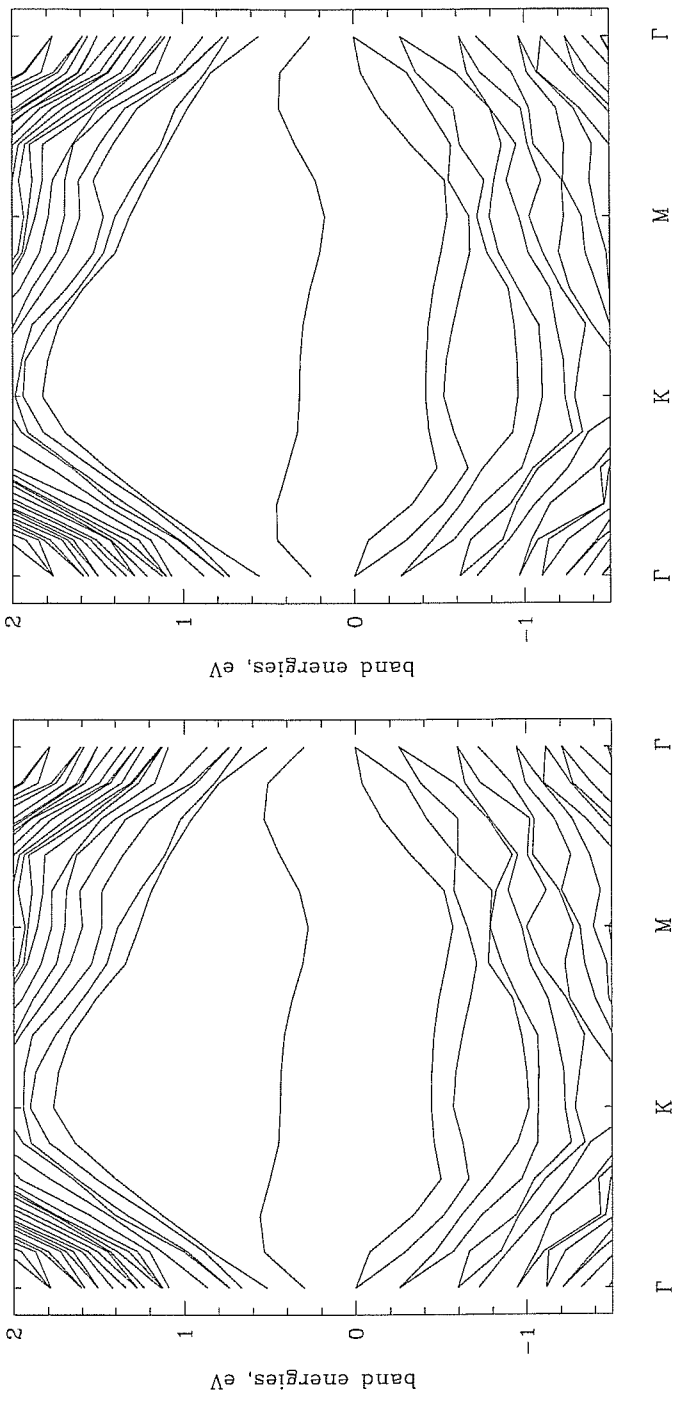

Figure 3.4: (a) Sn-Ge 2 × 2 electron bands; (b) Ge 2 × 2 ones. The region around the Fermi energy is shown. Plots are rotated to allow a better comparison.

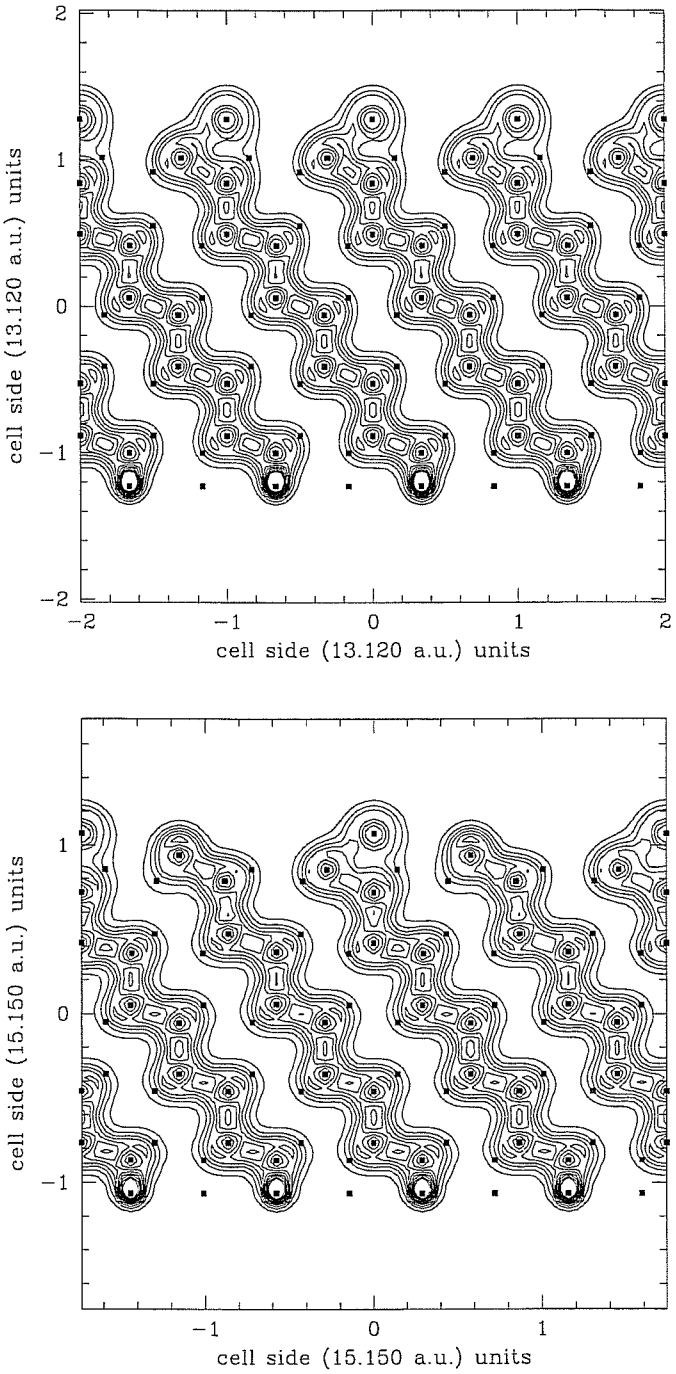

Figure 3.5: Charge density of: (a) the Sn-Ge $\sqrt{3}$ slab; (b) the Sn-Ge 2×2 slab. Densities are plotted on a vertical plane through adatoms and (for the 2×2 case) rest atoms. Positions of atoms near this plane are also shown.

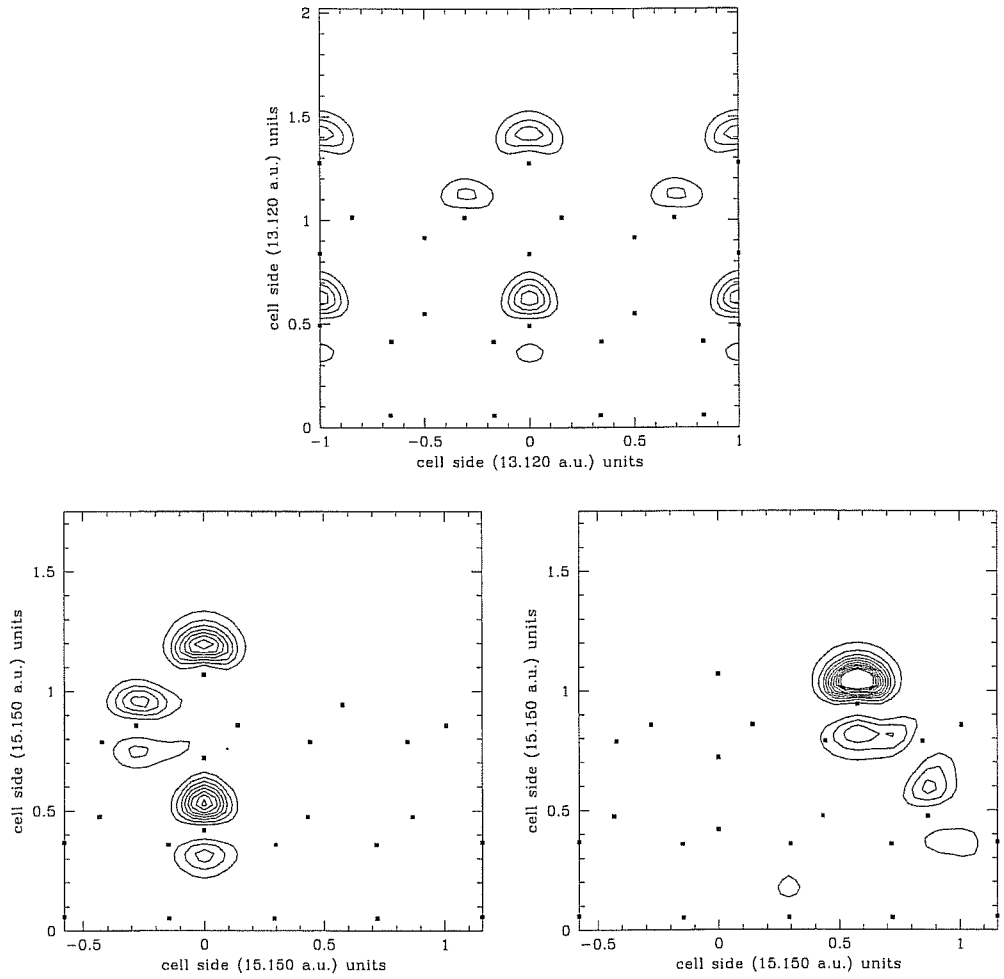

Figure 3.6: Charge density of: (a) the Sn-Ge $\sqrt{3}$ surface state (half-filled); (b) the Sn-Ge 2×2 higher surface state (empty); (c) the Sn-Ge 2×2 lower surface state (filled). Densities are calculated assuming all states fully occupied, and plotted on a vertical plane through adatoms and (for the 2×2 case) rest atoms. Positions of atoms near this plane are also shown.

3.3 Summary and conclusions

In this work we have calculated the free energies of four competing reconstructions of the Sn-Ge(111) surface. Our calculations have shown that an accurate Brillouin-zone integration is required to obtain reliable results; for our unit cells, the 6-k-points set of [6] gave good results. This set should be good (even better) also for larger units cells, which have a smaller IBZ, while smaller cells (e.g., 1×1 ones) may require a greater accuracy.

Our results imply that of those reconstructions, only the Sn-Ge $\sqrt{3}$ and the Ge 2×2 are stable phases of the system. The Sn-Ge 2×2 reconstruction appears not to be a stable phase; however, it may exist as a metastable one. In fact, experiments also point to this direction.

Our results agree with the experimental evidence that the Sn-Ge $\sqrt{3}$ phase, despite its being metallic and having half-filled dangling bonds, has a sufficiently low energy to prevail over the Sn-Ge 2×2 one; this is not true for the corresponding Ge phases. We suppose that the larger size of Sn atoms with respect to Ge ones play a major role in this phenomenon: the greater bond lengths imposed by Sn adatoms being so large cause the bond angles to increase, thus modifying the hybridization state and lowering the adatom's dangling-bond band. This mechanism, indeed, favours the $\sqrt{3}$ reconstruction against the 2×2 one.

This interpretation is supported by experimental observations on other (111)-surface systems: surfaces in which the adatom is larger than bulk atoms, such as the Pb-Ge(111) and the Pb-Si(111) ones, also reconstruct with a $\sqrt{3}$ structure [31, 32, 33, 34], while surfaces with equal-size (and possibly smaller) adatoms, such as clean Ge(111) and Si(111), don't. (Si(111) actually reconstructs with a larger, namely 7×7, structure; however, this is made of building blocks having an adatom-rest atom structure [35] as in the 2×2 reconstruction.)

Bibliography

[1] P. Hohenberg and W. Kohn. Inhomogeneous electron gas. *Physical Review, 2nd series*, 136(3B):864–871, november 9, 1964.

[2] W. Kohn and L.J. Sham. Self-consistent equations including exchange and correlation effects. *Physical Review, 2nd series*, 140(4A):1133–1138, november 15, 1965.

[3] L.J. Sham and W. Kohn. One-particle properties of an inhomogeneous interacting electron gas. *Physical Review, 2nd series*, 145(2):561–567, may 13, 1966.

[4] J. Ihm, Alex Zunger, and Marvin L. Cohen. Momentum-space formalism for the total energy of solids. *Journal of Physics C: solid state physics*, 12:4409–4422, 1979.

[5] D.J. Chadi and Marvin L. Cohen. Special points in the Brillouin zone. *Physical Review B*, 8(12):5747–5753, december 15, 1973.

[6] S.L. Cunningham. Special points in the two-dimensional Brillouin zone. *Physical Review B*, 10(12):4988–4994, december 15, 1974.

[7] D.R. Hamann, M. Schlüter, and C. Chiang. Norm-conserving pseudopotentials. *Physical Review Letters*, 43(20):1494–1497, november 12, 1979.

[8] Leonard Kleinman and D.M. Bylander. Efficacious form for model pseudopotentials. *Physical Review Letters*, 48(20):1425–1428, may 17, 1982.

[9] G.B. Bachelet, D.R. Hamann, and M. Schlüter. Pseudopotentials that work: from H to Pu. *Physical Review B*, 26(8):4199–4228, october 15, 1982.

[10] D.M. Ceperley and B.J. Alder. Ground state of the electron gas by a stochastic method. *Physical Review Letters*, 45(7):566–569, august 18, 1980.

[11] J.P. Perdew and Alex Zunger. Self-interaction correction to density-functional approximations for many-electron systems. *Physical Review B*, 23(10):5048–5079, may 15, 1981.

[12] Lu Zhong-Yi. *First-principles study of α-Sn surfaces.* PhD thesis, SISSA/ISAS Scuola Internazionale Superiore di Studi Avanzati/ International School for Advanced Studies, Trieste, october 1996.

[13] Ernest R. Davidson. Super-matrix methods. *Computer Physics Communications*, 53:49–60, 1989.

[14] D.D. Johnson. Modified Broyden's method for accelerating convergence in self-consistent calculations. *Physical Review B*, 38(18):12807–12813, december 15, 1988.

[15] John E. Northrup. Origin of surface states on Si(111)(7 × 7). *Physical Review Letters*, 57(1):154–157, july 7, 1986.

[16] John E. Northrup and J. Neugebauer. Theory of the adatom-induced reconstruction of the SiC(0001) $\sqrt{3} \times \sqrt{3}$ surface. *Physical Review B*, 52(24):17001–17004, december 15, 1995.

[17] Magdalena Sabisch, Peter Krüger, and Johannes Pollmann. Ab-initio calculations of structural and electronic properties of 6H-SiC(0001) surfaces. *Physical Review B*, 55(16):10561–10570, april 15, 1997.

[18] Silvio Modesti. Private communication.

[19] D.J. Chadi and C. Chiang. New c-2 × 8 unit cell for the Ge(111) surface. *Physical Review B*, 23(4):1843–1846, february 15, 1981.

[20] R.S. Becker, J.A. Golovchenko, and B.S. Swartzentruber. Tunneling images of germanium surface reconstructions and phase boundaries. *Physical Review Letters*, 54(25):2678–2680, june 24, 1985.

[21] Toshihiro Ichikawa and Shozo Ino. Structural study of Sn-induced superstructures on Ge(111) surfaces by RHEED. *Surface Science*, 105:395–428, 1981.

[22] H. Sakurai, K. Higashiyama, S. Kono, and T. Sagawa. X-ray photoelectron diffraction study of the atomic geometry of the Ge(111)($\sqrt{3} \times \sqrt{3}$)R30^0-Sn surface. *Surface Science Letters*, 134:550–556, 1983.

[23] M. Göthelid, M. Hammar, C. Törnevik, U.O. Karlsson, N.G. Nilsson, and S.A. Flodström. Sn-induced surface reconstructions on the Ge(111) surface studied with scanning tunneling microscopy. *Surface Science Letters*, 271:357–361, 1992.

[24] M. Göthelid, T.M. Grehk, M. Hammar, U.O. Karlsson, and S.A. Flodström. Adsorption of tin on the Ge(111)-c(2×8) surface studied with scanning tunneling microscopy and photoelectron spectroscopy. *Surface Science*, 328:80–94, 1995.

[25] G. Le Lay, V.Yu. Aristov, O. Boström, J.M. Layet, M.C. Asensio, J. Avila, Y. Huttel, and A. Cricenti. Surface charge density waves at Sn/Ge(111)? *Applied Surface Science*, 123/124:440–444, 1998.

[26] David R. Lide, editor. *CRC handbook of chemistry and physics.* CRC Press, Boca Raton, Florida, 74th edition, 1994.

[27] A. Baldereschi. Mean-value point in the Brillouin zone. *Physical Review B*, 7(12):5212–5215, june 15, 1973.

[28] Qian Guo-Xin, Richard D. Martin, and D.J. Chadi. First-principles study of the atomic reconstructions and energies of Ga- and As-stabilized GaAs(100) surfaces. *Physical Review B*, 38(11):7649–7663, october 15, 1988.

[29] John E. Northrup and Sverre Froyen. Energetics of GaAs(100)-(2 × 4) and -(4 × 2) reconstructions. *Physical Review Letters*, 71(14):2276–2279, october 4, 1993.

[30] Walter Ashley Harrison. *Electronic structure and the properties of solids. The physics of the chemical bond.* Dover Publications, inc., New York, 1989.

[31] J.A. Carlisle, T.Miller, and Chiang T.-C. Photoemission study of the growth, desorption, Schottky-barrier formation, and atomic structure of Pb on Si(111). *Physical Review B*, 45(7):3400–3409, february 15, 1992.

[32] J.A. Carlisle, T.Miller, and Chiang T.-C. Photoemission study of Pb on Ge(111). *Physical Review B*, 47(7), february 15, 1993.

[33] Joseph M. Carpinelli, Hanno H. Weitering, E. Ward Plummer, and Roland Stumpf. Direct observation of a surface charge density wave. *Nature*, 381:398–400, may 30, 1996.

[34] G. Le Lay. Surfaces et interfaces prototypes du silicium et du germanium. *Journal de Physique IV*, 7:115–125, december 1997.

[35] Kunio Takayanagi, Yasumasa Tanishiro, Shigeki Takahashi, and Masaetsu Takahashi. Structure analysis of Si(111)-7×7 reconstructed surface by transmission electron diffraction. *Surface Science*, 164:367–392, 1985.